Sex-dependent neural plasticity in response to damage

Marina Recatalà-Martinez[1], Manel Bosch[2], Pedro Gaspar[3], Alessandro Mineo[3], Santiago Rios[1], Irene Miguel-Aliaga[3], Marta Morey[1,4,*]

1.Departament de Genètica, Microbiologia i Estadística, Facultat de Biologia, Universitat de Barcelona, Barcelona, Spain

2. Unitat de Microscòpia Òptica Avançada, Centres Científics i Tecnològics de la Universitat de Barcelona (CCiTUB), Barcelona, Spain

3. The Francis Crick Institute, London, United Kingdom.

4. Human Genetics and Disease, Institut de Biomedicina de la Universitat de Barcelona (IBUB), Barcelona, Spain

*Corresponding author: mmorey@ub.edu

ABSTRACT

Plasticity of intact neural tissue in the vicinity of neural damage serves to restoring functionality of circuits. Much remains to be learned about the mechanisms regulating this process and the reported sex differences in recovery outcomes. Here we present the fly gut and its innervation as simplified model to address these questions. We show that gut damage caused by ingestion of toxic agents resulted in plasticity of the enteric neuronal network, manifested as a Reactive Oxygen Species (ROS)-dependent increase in neural tissue, which was reversible after a recovery period. Interestingly, males did not display neural plasticity, and masculinization of neurons in females suppressed the damage-dependent neural growth. Together, these findings position the fly gut as a system to investigate the cellular, molecular and sex-specific underpinnings of neural plasticity, with implications for therapeutic advancements in neural circuit recovery.

INTRODUCTION

Neural plasticity involves two key mechanisms for recovery after injury: axonal regeneration and structural plasticity of intact neural tissue. While axonal regeneration has been widely studied (Mahar and Cavalli, 2018; Tedeschi and Bradke, 2017),

modulating the plasticity of remaining healthy neural tissue offers an alternative route to restore function (Gao et al., 2022; Petersen et al., 2022). Clinical evidence shows that this form of plasticity supports functional recovery and circuit reorganization after acute damage such as stroke (Cirillo et al., 2020; Murphy and Corbett, 2009; Nudo, 2003; Sampaio-Baptista et al., 2018) or multiple sclerosis episodes (Ksiazek-Winiarek et al., 2015; Prosperini et al., 2015). Notably, recovery outcomes show sex-specific differences, (Turtzo and McCullough, 2008; Yu et al., 2015), suggesting variability in plasticity capacity (Hyer et al., 2018; Kirby et al., 2024).

Despite these observations, the molecular mechanisms regulating plasticity in intact adult neural tissue remain poorly understood. This is partly due to the technical challenges of studying healthy and damaged neurons in close proximity, which make it difficult to isolate and study specific structural plasticity processes. To address this, we developed a model that focuses on how intact neurons respond to non-neural tissue damage, using peripheral innervation as an accessible system. This allows for controlled injury and analysis of plasticity in a physiologically relevant yet simplified context.

We used the digestive tract of *Drosophila melanogaster* as a model system. Like in mammals, the fly gut is structurally and functionally compartmentalized (Buchon et al., 2013; Lemaitre and Miguel-Aliaga, 2013; Marianes and Spradling, 2013). Its epithelium includes intestinal stem cells (ISCs), enteroblasts (EBs), absorptive enterocytes (ECs), and secretory enteroendocrine (EE) cells. The gut is wrapped in muscle, oxygenated by a tracheal system, and innervated by neurons located in the central nervous system, the corpora cardiaca (neurosecretory structure), and the hypocerebral ganglion (HCG, one of the stomatogastric ganglia) (Kuraishi et al., 2015; Miguel-Aliaga et al., 2018). While most neurites target visceral muscle, some extend to the underlying epithelium (Cognigni et al., 2011; Cui et al., 2024; Kenmoku et al., 2016; Petsakou et al., 2023). Unlike mammals, innervation in the fly gut is regionally restricted, making it well-suited for targeted analysis (Kuraishi et al., 2015; Miguel-Aliaga et al., 2018). Recent studies reveal that gastrointestinal neurons respond to factors such as microbiota, nutrients, aging, and reproductive state in flies and mammals (Ameku et al., 2020; Hadjieconomou et al., 2020). While functional plasticity has been observed in the posterior fly midgut during

recovery (Petsakou et al., 2023), the mechanisms of structural plasticity in response to gut damage—and how they are shaped by biological sex—remain unexplored. Here, we show that intact neurons innervating the anterior midgut exhibit a female-specific, ROS-dependent reversible structural plasticity, which is absent in male flies and suppressed in females with masculinized neurons.

RESULTS AND DISCUSSION

Intestinal damage induces reversible neural plasticity.

In order to quantify and characterize the innervation in the anterior part of the midgut we proceeded to select a neural driver and reporter that would specifically label neuronal processes with native GFP fluorescence. This prevented background signal from secondary antibodies and provided a high signal to noise ratio which facilitated faithful neural process quantification as GFP signal. General neuronal markers, such as Elav (Chen et al., 2016; Holsopple et al., 2022; Titos et al., 2023) or n-Synaptobrevin (Weaver et al., 2020), also label EEs. However, we used the *GMR51F12-GAL4* driver line from the Janelia FlyLight collection (Jenett et al., 2012; Min et al., 2021; Olds and Xu, 2014) and a specific *nSyb.S-GAL4* driver (Weaver et al., 2020), neither of which labels EEs. Morphological landmarks in whole-mount preparations, combined with phalloidin co-staining to visualize the surrounding musculature, enabled consistent imaging of the same digestive tract region and its associated neural innervation (Figure 1A). Using 3D reconstruction and image analysis we obtained volume quantifications for both the digestive tube and neural tissue (see Materials and Methods). Scaling growth is a prevalent phenomenon in the peripheral nervous system where sensory and motor neurons must adjust the size of their arborizations according to the area of their target tissues to maintain their functionality (Bentley and Toroian-Raymond, 1981; Bucher and Pflüger, 2000; Lee and Stevens, 2007; Menon et al., 2013). Measuring the volume of the digestive tube enabled us to use statistical analysis methods that accounted for and removed any potential influence of digestive tube size variation in adults (driven by treatment or genetic background) on neural tissue quantification comparisons (see Materials and Methods).

To damage the gut we fed flies with DSS. DSS is a polymer that induces colitis in mammals (Yang and Merlin, 2024) and has been used in *Drosophila* to study the cellular mechanisms and molecular pathways that regulate ISC proliferation during regeneration (Jiang et al., 2016; Tian et al., 2022). When flies ingest DSS it crosses the epithelium expanding the basement membrane sheet and altering muscle morphology (Howard et al., 2019). The resulting change in biomechanical forces in the niche is thought to activate ISC division (Howard et al., 2019). DSS feeding also results in trachea sprouting (Perochon et al., 2021), which is necessary for ISC proliferation (Perochon et al., 2021; Tamamouna et al., 2021). Interestingly, basement membrane and muscle defects, as well as trachea remodeling, are reversible after a recovery period (Howard et al., 2019; Perochon et al., 2021; Tamamouna et al., 2021). We wondered whether adult neurons were plastic and could also respond to gut damage.

To analyze the effect of gut damage on neural plasticity we fed adult mated females with DSS for 4 days and compared them to controls fed with the carrier (sucrose). We confirmed the effectiveness of DSS by replicating previously published observations, including a reduction in lifespan (Amcheslavsky et al., 2009) (data not shown) and an increase in the proliferative response of ISCs in the midgut (Amcheslavsky et al., 2009) (see later in Figure 2A). Over 90% of the flies that survived the feeding protocol tested negative for the SMURF assay (Rera et al., 2012), indicating that in the majority of animals (93,3%±SD4.5) that were dissected gut permeability was not compromised. Thus, during DSS feeding, neurons were largely shielded from direct exposure to gut contents that could potentially cause them damage. When we dissected the DSS-fed females and compared them to control flies we observed a significant increase in neural tissue (Figure 1B). To rule out neurogenesis as the source of the new neural tissue, we quantified the number of neural nuclei in the HCG, the primary source of neurons innervating the anterior midgut (Figure 1A). No differences were observed between control and DSS-fed animals (Figure 1C), suggesting that the increase in neural tissue was due to neural growth. This neural growth was not exclusive to DSS damage since we also observed it when feeding the flies with H_2O_2 (Figure 1D).

Figure 1

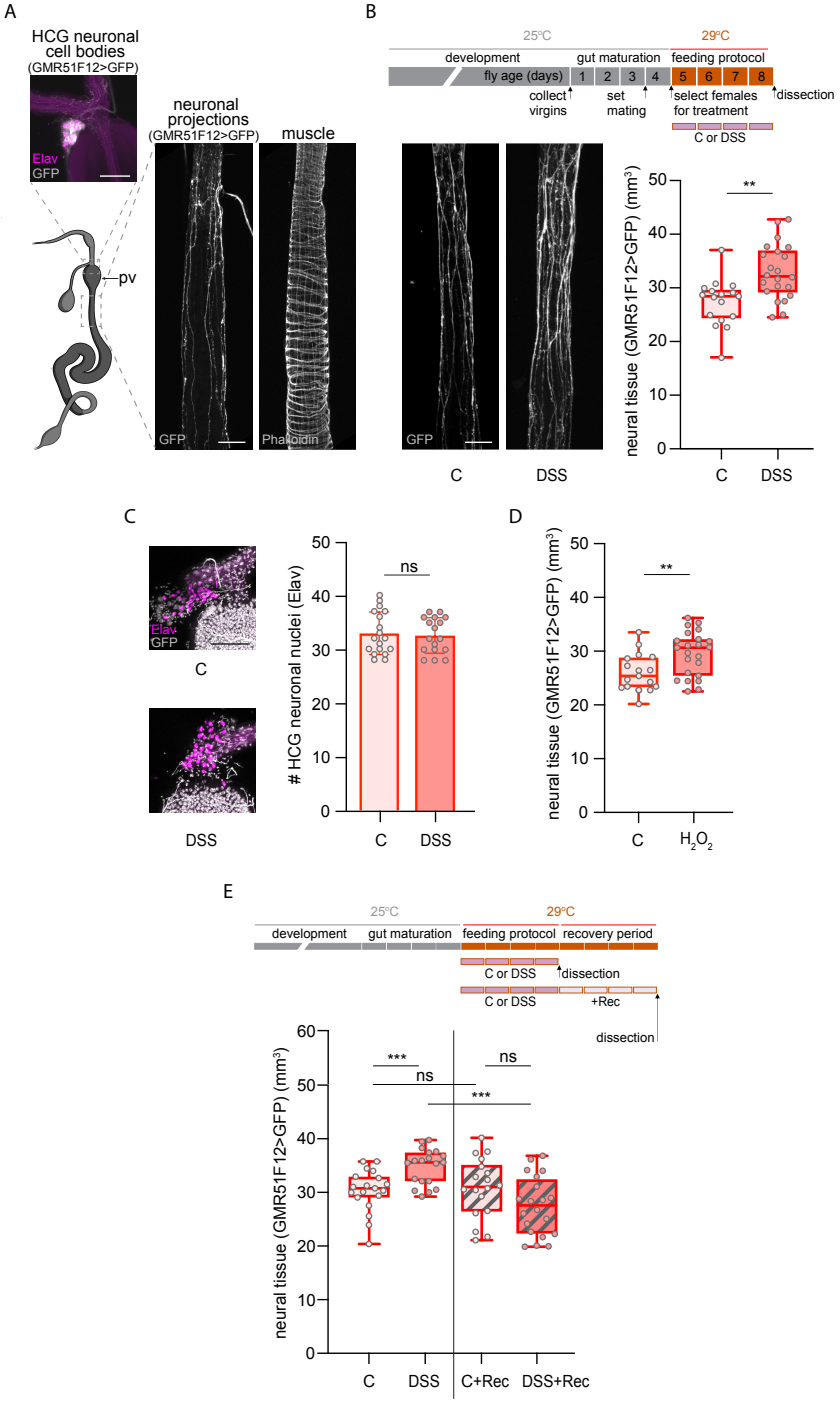

Figure 1. Neural plasticity induced by gut damage resolves after recovery. A) Drawing of the adult gut with two areas of interest highlighted and corresponding confocal Z-projections. The square box region corresponds to the area above the proventriculus (pv) and the image shows neuronal nuclei (magenta, anti-Elav) and neuronal membrane (grey, GFP) of the HCG. Autofluorescence of the peritrophic membrane lining the gut in this

135 region is observed. The rectangular box region corresponds to the area of the anterior
136 midgut imaged in subsequent analysis and the images show neuronal processes (grey,
137 GFP) and muscle fibers (grey, Phalloidin). B) Schematic outlining the feeding protocol and
138 dissection time. Confocal Z-projections of neuronal processes innervating the anterior
139 midgut of control (C) and DSS-fed (DSS) females and quantification of neural tissue. Red
140 outline in the box plots or bar graphs indicates female. C) Confocal Z-projections of the
141 HCG of control and DSS-fed females stained with Hoechst (grey, which also accumulates
142 in some tracheal branches) and showing neuronal nuclei (magenta, anti-Elav).
143 Quantification of neuronal nuclei in the HCG of C and DSS-fed females. D) Quantification
144 of neural tissue in control and H_2O_2-fed females. E) Schematic of the feeding protocol
145 and recovery period. Quantification of neural tissue after the feeding protocol and after
146 the recovery period (Rec). Scale bar 50µm. Statistical significance is indicated as follows:
147 * $p < 0.05$, ** $p < 0.01$, *** $p < 0.001$, n.s = not significant. Gut schematic from
148 *BioRender.com*.
149
150 Tracheal terminal cells (TTCs) sprout in response to DSS and H_2O_2 (Perochon et al., 2021;
151 Tamamouna et al., 2021), so we examined their behavior in the anterior midgut. This
152 region showed sparse tracheation, which remained unchanged after DSS feeding,
153 indicating that TTCs in this area were unresponsive to gut damage (Supplementary Figure
154 1A, B). Moreover, TTC morphology did not match the extent of neural growth, suggesting
155 they do not serve as a scaffold for neural tissue growth in this area.
156
157 We next explored the stability of this neural plasticity and conducted recovery
158 experiments (Figure 1E). While DSS feeding increased the neural tissue (C versus DSS), a
159 4-day recovery period (DSS + Rec) reverted the amount of neural tissue to levels as those
160 of control flies (C + Rec). Consistent with this observation, a clear reversal of neural
161 growth was observed when comparing flies dissected after the DSS treatment (DSS) and
162 those dissected after the recovery phase (DSS + Rec). No differences were observed
163 between control flies (C versus C + Rec).
164
165 In summary, these experiments indicate that the intact neural tissue innervating the
166 digestive tube is plastic and responds to damage with growth. This neural growth is

167 reversible after a recovery period, as the gut returns to homeostasis after injury.
168 Importantly, these observations were validated with two independent neural drivers
169 (*GMR51F12-GAL4*, Figure 1 and *nSyb.S-GAL4*, Supplementary Figure 1C).
170
171 **ISC proliferation does not mediate neural plasticity.**
172 To determine whether ISC proliferation drove DSS-induced neural growth, we first
173 confirmed that DSS feeding increased ISC division in the anterior midgut, as shown by
174 elevated Histone H3 phosphorylation (H3P) signal and lineage tracing using ReDDM
175 (Antonello et al., 2015) (Figures 2A–B) (see Materials and Methods). To test causality, we
176 blocked ISC cell division during DSS feeding using a combination of a *Cdk1* null allele
177 ($Cdk1^{null}$) and a temperature-sensitive allele ($Cdk^{1E1–24}$) (Rodríguez et al., 2024) (Figure 2C).
178 Neural growth remained unaffected by the proliferation block (Figure 2D), indicating that
179 ISC division is not required for DSS-induced neural plasticity.
180
181 **Gut-derived ROS stimulates neural plasticity.**
182 DSS feeding results in epithelial damage, causing cell death and an increase in ROS
183 levels (Wu et al., 2012). To test the contribution of ROS levels to neural growth, we co-fed
184 flies with DSS and the ROS inhibitor N-acetyl cysteine (NAC). Neural growth was reduced
185 in DSS + NAC flies and comparable to control + NAC levels (Figure 2E), indicating that
186 DSS-dependent ROS promotes neural plasticity.
187
188 **Reversal of neural growth as the gut returns to homeostasis is not caspase**
189 **dependent.**
190 We were curious about the mechanisms controlling neural growth reversal during
191 recovery. Axon pruning can take place either through axon retraction or degeneration (Luo
192 and O'Leary, 2005). During developmental remodeling dendritic arborizing (da) sensory
193 neurons ddaC degenerate (Williams and Truman, 2005) using local caspase activation to
194 direct dendrite engulfment (Williams et al., 2006). To assess whether caspases mediated
195 neural growth reversal, we inhibited apoptosis in neurons by overexpressing Diap1.
196 Reversal still occurred (Supplementary Figure 2), suggesting that this process may result
197 from axon retraction rather than caspase-dependent mechanisms.
198

Figure 2

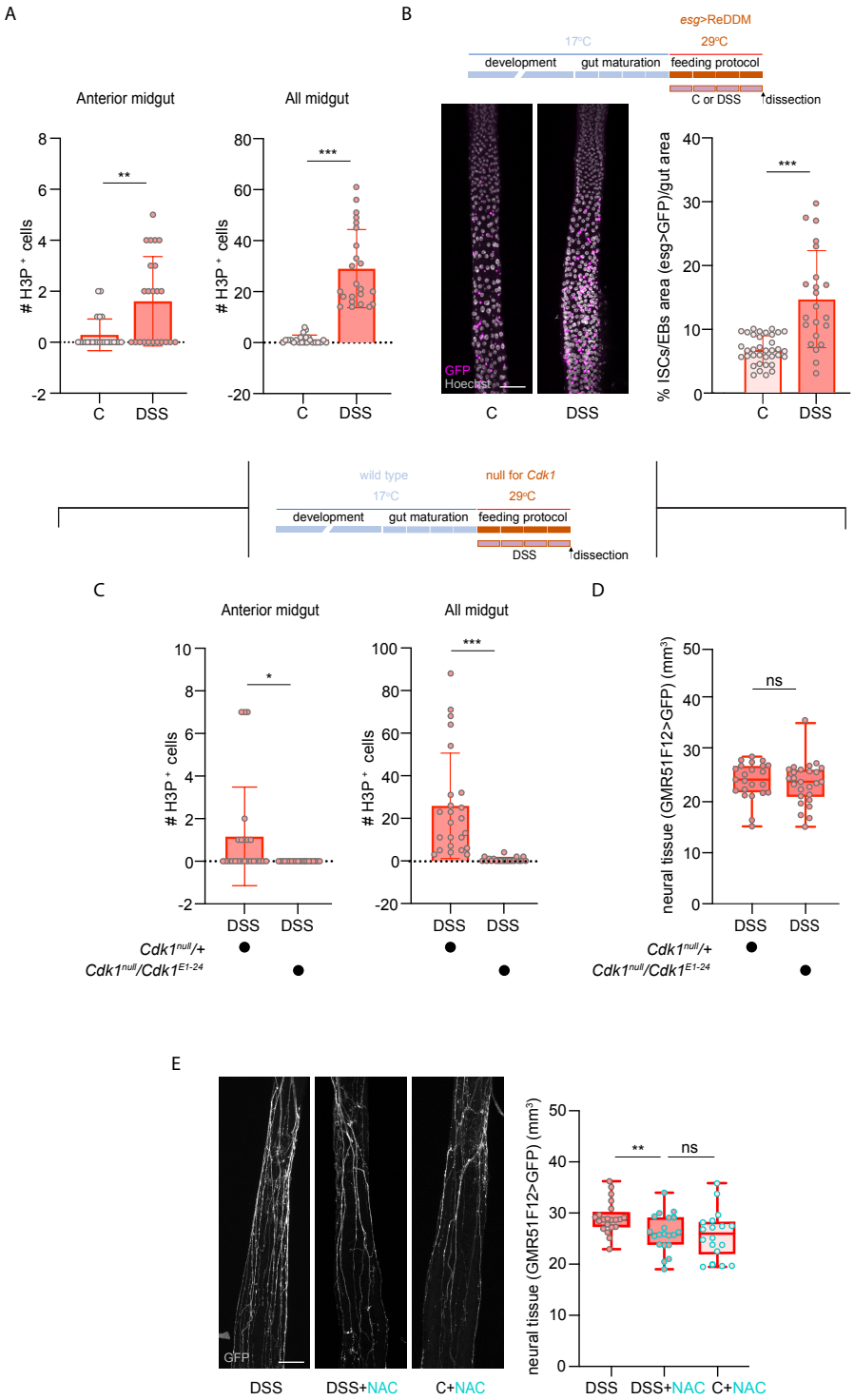

Figure 2. Neural plasticity does not depend on ISC proliferation but on gut-derived ROS. A) Quantification of H3P/Hoechst positive cells in the anterior and the whole midgut in C and DSS-fed females. B) Schematic showing activation of ReDDM lineage tracing during the feeding protocol. Confocal Z-projections of the anterior midgut stained with

205 Hoechst (grey) and showing the cell membrane of ISCs/EBs (magenta, anti-GFP) in C and
206 DSS-fed females. Quantification of the percentage of the ISC/EB area (GFP signal) from
207 the total area of the anterior mid gut in C and DSS-fed females. C-D) Schematic showing
208 temperature dependent knock out of Cdk1 function during the feeding protocol. C)
209 Quantification of H3P/Hoechst positive cells in the anterior midgut and the whole midgut
210 in wild type (heterozygous) and *Cdk1* null females after DSS feeding. D) Quantification of
211 neural tissue in wild type and *Cdk1* null females after DSS feeding. E) Confocal Z-
212 projections of neuronal processes in the anterior midgut of DSS, DSS + NAC and C +NAC
213 -fed females and quantification of neural tissue. Scale bar 50µm. Statistical significance
214 is indicated as follows: $*\, p < 0.05$, $**\, p < 0.01$, $***\, p < 0.001$, n.s = not significant.
215
216 **Neural plasticity is exclusive to females and is actively suppressed when female**
217 **neurons are masculinized.**
218 Interestingly, males did not exhibit neural growth following DSS treatment (Figure 3A). To
219 investigate whether this neural growth was exclusive to female neurons, we aimed to
220 create female individuals with masculinized neurons. Most sex differences in *Drosophila*
221 arise from the female specific expression of the *Sex lethal* gene (*Sxl*) which codes for an
222 RNA binding protein (Bell et al., 1988). Sxl induces the alternative splicing of the
223 *transformer* (*tra*) gene generating the female fate determining TraF protein only in females
224 (Belote et al., 1989; Boggs et al., 1987; Inoue et al., 1990; Sosnowski et al., 1989). We first
225 confirmed that neurons in the HCG expressed the female-specific alternative splicing
226 variant of *tra* while males didn't (Figure 3B,C) (Hérault et al., 2024). Subsequently, we
227 proceeded to masculinize neurons in females by means of *tra* downregulation with RNAi
228 during development (Figure 3D). We confirmed that the presence of the *UAS-Dcr2*
229 transgene did not affect the response of wild type females to DSS, and thus, the expected
230 increase in neural tissue was observed. Interestingly, DSS feeding did not have any effect
231 in masculinized females and the amount of neural tissue was not significantly different
232 between control and DSS-fed flies. In addition, DSS-fed masculinized females displayed
233 significantly less neural tissue that DSS-fed control flies, aligning with the absence of
234 neural growth in masculinized females.
235

Figure 3

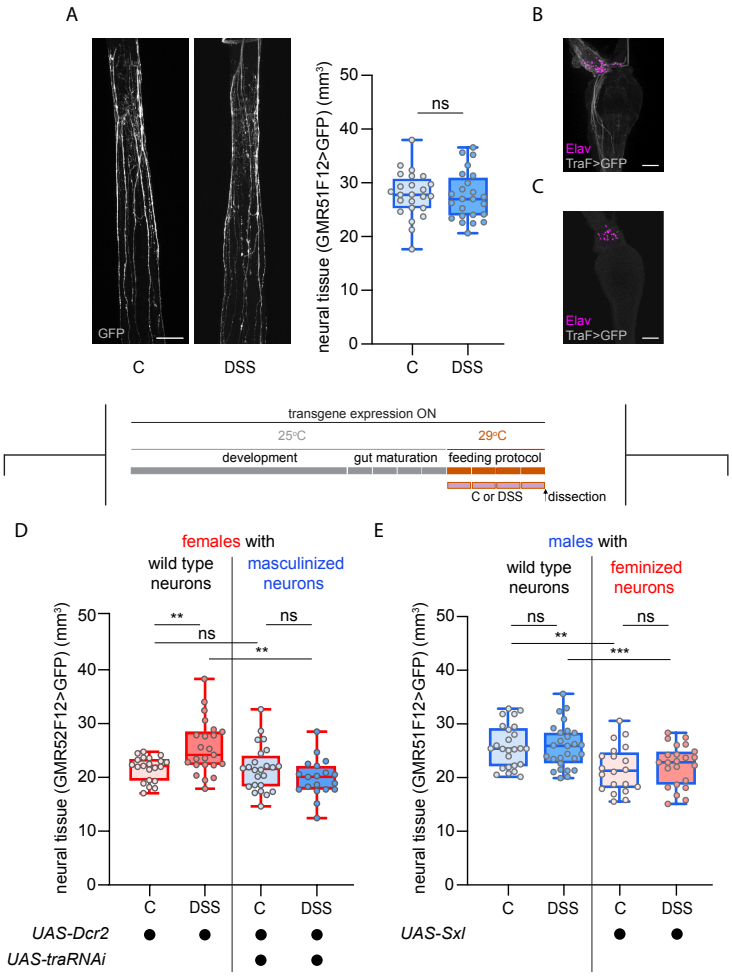

236

237

238 ***Figure 3.*** **Neural plasticity is not observed in males and masculinization of female**
239 **neurons abolishes neural growth.** A) Confocal Z-projections of neuronal processes in
240 the anterior midgut of C and DSS-fed males, and quantification of neural tissue. Blue
241 outline in box plots indicates male. B-C) Confocal Z-projections at the level of the HCG
242 showing female-specific *tra* alternative splicing in neurons (grey, GFP; magenta, Elav) in
243 females (B) and absence in males (C). D-E) Schematic showing transgene expression in
244 neurons in relation to the feeding protocol. D) Quantification and comparison of neural
245 tissue in females and females with masculinized neurons both in C versus DSS-fed
246 conditions. E) Quantification and comparison of neural tissue in males and males with
247 feminized neurons both in C versus DSS-fed conditions. Scale bar 50µm. Statistical
248 significance is indicated as follows: * $p < 0.05$, ** $p < 0.01$, *** $p < 0.001$, n.s = not
249 significant.

We also carried out the reverse experiment and attempted to confer plasticity to male neurons by feminizing them through developmental *Sxl* overexpression (Figure 3E) (Bell et al., 1991). In this case, the DSS treatment had no effect in feminized males, and we did not observe the neural growth we expected to see for a successfully feminized male. Moreover, both control and DSS-fed feminized males showed less amount of neural tissue than wild type males. These results indicate that neuronal Sxl overexpression in males is not sufficient to induce damage-responsive plasticity, and may even impair neural tissue growth in our context.

These findings reveal a previously unrecognized sex-specific mechanism of neural plasticity in the fly gut, where female neurons exhibit a unique capacity for damage-induced growth that is actively suppressed by masculinization. In addition, the lack of neural growth in males following DSS-induced gut damage suggests that neural plasticity is limited in males compared to females.

The *Drosophila* gut and its innervation as a model to investigate neural plasticity and the role of sex in its regulation

This system enables the study of both structural growth and retraction phases of adult intact neural tissue in response to damage, capturing the dynamic nature of plasticity. In addition, we uncovered a clear sexual dimorphism: neural growth is absent in males and suppressed in masculinized female neurons. However, feminizing male neurons was not sufficient to induce plasticity. Two key avenues emerge for understanding this dimorphism. First, our findings suggest that sex-specific gene expression may underlie the observed differences in plasticity, pointing to differentially expressed genes as potential regulators of neural responsiveness. We show that DSS-induced ROS promotes neural growth in females, aligning with evidence that ROS supports structural plasticity (Oswald et al., 2018). Sex differences in gene expression regulating ROS production or in ROS-responsive signaling pathways, such as TOR and InR/PI3K/Akt, which regulate neural regrowth during developmental remodeling in flies (Sanal et al., 2023; Yaniv and Schuldiner, 2016) and mammalian regeneration (Lund-Ricard et al., 2020), could drive the female-specific neural growth observed in response to gut damage. Second, the

failure of feminized male neurons to elicit growth implies that neuronal identity alone is not enough—sex-specific cues from surrounding tissues such as the gut epithelium, visceral muscle, or tracheal cells may be necessary to support or trigger neural growth. Similarly, during recovery, axon retraction could involve cell surface molecules like Ephrins, Slits or Semaphorins, potentially expressed by female-specific gut tissues, akin to repulsive axon guidance mechanisms (Luo and O'Leary, 2005).

Building on evidence that sex influences organ formation and physiology (Mank and Rideout, 2021), the results presented here establish the *Drosophila* gut and its innervation as a model for elucidating how sex shapes neural plasticity of intact neural tissue in response to damage. Understanding these mechanisms could guide the development of sex-specific therapeutic strategies for neural repair.

MATERIALS AND METHODS

Fly stocks

The following fly lines were used: *GMR51F12-GAL4* (BDSC:58685), *nSyb-GAL4.S* (BDSC: 51635), *UAS-Flybow.1.1B* (used as 10xUAS-CD8::GFP, BDSC: 56802, 56803), *DSRF.Term-GAL4* (BDSC: 25753), *esg-GAL4* (a gift from M. Milán, unknown insertion), *UAS-mCD8::GFP* (BDSC:5130), *UAS-H2B::RFP* (a gift from J. Morante), *tubP-GAL80*^{ts} (BDSC: 7017), *Cdk1*^{null} (BDSC: 6643), *Cdk*$^{1E1–24}$ (BDSC: 6641), *UAS-Diap1* (BDSC: 15310), *traF-GAL4* (a gift from B. Hudry), *UAS-Dcr-2* (BDSC: 24650), *UAS-traRNAi.TRiPJF03132* (*UAS-traRNAi*, BDSC: 28512), *UASp-Sxl.alt5-C8* (*UAS-Sxl*, BDSC: 58484). The list of complete genotypes is available in Supplementary Information.

Feeding protocols

For feeding assays, virgin females were collected and aged on standard media at 25°C for 3-4 days before undergoing mating for 24hrs. Then same procedure was carried out when experiments were performed with males. Flies were recovered from the mating and transferred in groups of 10 to an empty vial containing 5 pieces of 2cm × 2cm of bench paper soaked with 500ml of the desired feeding solution. Flies were transferred to a new vial with fresh feeding paper every day for the specified number of days prior to dissection. The feeding protocol was always done at 29°C. For DSS (Merck, 42867)

314 induced damage, flies were fed with 5% sucrose (Control) or with 6% DSS in 5% sucrose
315 (DSS) for 4 days. For the SMURF assay, the last control and DSS feeding solutions prior to
316 the day of dissection were laced with Brilliant Blue FCF (80717, Merck) at 2.5% w/v. For
317 H_2O_2 (1072100250, Merck) induced damage, flies were fed with 5% Sucrose (Control) or
318 1% H_2O_2 in 5% sucrose (H_2O_2) for 4 days. For NAC treatment, flies were fed with 1,2mM
319 NAC in 5% sucrose (Control + NAC) or 6% DSS + 1,2mM NAC in 5% sucrose (DSS + NAC)
320 for 4 days. For recovery protocols, after the DSS feeding protocol, control and DSS-fed
321 flies were each transferred to vials with 5% sucrose for 4 days (Control + Recovery; DSS
322 + Recovery). To carry out comparisons within the same cohort of flies, a subset of flies
323 was dissected after the DSS treatment and the rest after the recovery period.
324
325 **Temperature sensitive assays**
326 To visualize the amount of proliferation taking place exclusively during the four days of
327 the feeding protocol we set ReDDM-based crosses (Antonello et al., 2015). This lineage
328 tracing approach uses the Gal80 temperature sensitive allele (*Gal80*^{ts}), which inhibits
329 GAL4 transcription at permissive temperature (19ºC) and allows it at the restrictive one
330 (29ºC) (McGuire et al., 2003), and *esg-GAL4* to label ISCs and EBs. Crosses were grown
331 and flies were kept at 17°C to ensure Gal80^{ts} repression until adult mated female flies
332 were shifted to 29°C to inactive the Gal80 and carry out the feeding protocol. To block ISC
333 proliferation during the feeding protocol, *Cdk1*^{null}/ *Cdk*$^{1E1–24}$ flies were grown, aged and
334 mated at 17ºC, Cdk1 function was abrogated once the flies were transferred to 29ºC
335 (Rodriguez et al., 2024) during the DSS feeding protocol.
336
337 **Dissection and immunostaining**
338 To obtain the gut flies were dissected in PBS. Adult animals had their heads cut off with
339 scissors by the neck, their abdomens were pulled apart from the thorax and opened to
340 extract the gut. With this procedure the digestive tube was severed well above the crop
341 duct. Once fat and ovaries were removed, the gut was handled by its posterior end and
342 transferred to PBS in a well drawn onto a poly-l-lysine-coated slide (P1524, Merck) using
343 hydrophobic silicone (Flowsil, Intek Adhesives). In cases were the anterior part of the
344 midgut had to be repositioned, we manipulated the gut from the crop to avoid touching
345 the digestive tube. Guts were fixed at room temperature for 30min in 4% PFA in PBS.

346 Washes were done with PBS-T (PBS, 0.25% Triton X-100). To label the muscle or nuclei,
347 guts were incubated at room temperature for 30 min with Alexa Fluor™ 635 Phalloidin
348 (1/400, A34054, Invitrogen) or Hoechst 33258 (1/1000, H3569, Invitrogen) respectively in
349 PBS-T. A final wash with PBS was done prior to mounting. When antibodies were used,
350 primaries were incubated overnight at 4ºC, and secondaries were incubated at room
351 temperature for 2–3 h. The following antibodies were used: rat-anti-Elav (1/100, 7E8A10,
352 DSHB), rabbit-anti-H3P (1/1000, 06-570, EDM Milipore), rabbit-anti-DsRed (1/200,
353 632496, Clontech), chicken-anti-GFP (1/800, ab13970, Abcam), Alexa Fluor™ 568 goat-
354 anti-rat, Alexa Fluor™ 488 goat-anti-rabbit, Alexa Fluor™ 568 goat-anti-rabbit, Alexa
355 Fluor™ 488 goat-anti-chicken (1/500, A11077, A11008, A11011, A11039, Life
356 Technologies). Samples were mounted in VECTASHIELD® PLUS Antifade Mounting (H-
357 1900-10, Vector Laboratories).
358
359 **Microscopy**
360 Samples were imaged using a Zeiss LSM 880 confocal microscope (Zeiss, Germany)
361 equipped with a 25X 0.8 glycerol immersion media objective and an Argon and a
362 HeNe633 lasers. For neural network analysis, to consistently image the same region in
363 each gut, we used the end of the proventriculus as a positional landmark and captured
364 the gut section that fit within the visual field of the 25X objective at 0.8 magnification,
365 which in our set up generated images of 566,79 μm^2. As quality control for dissection,
366 only guts with an intact HCG were considered since this ganglion contains the cell bodies
367 of many of the neurons innervating the anterior midgut. Stacks of images were acquired
368 with a pixel size of 0.55x0.55x1um (xyz) and a pixel dwell time of 2.05us.
369
370 **Image processing and quantifications based on images**
371 Images were processed with Fiji (version ImageJ 1.53c, (Schindelin et al., 2012) and
372 figures assembled using Adobe Illustrator (Adobe, San Jose, CA).
373 *For quantification of neural tissue and gut parameters:* The channel with the neuron
374 staining was filtered in 3D (Ollion et al., 2013) first with the maximum filter and then with
375 the minimum one, with a radius of 3.3um in x and y and 2um in z, in both filters. Then the
376 filtered stack was processed using the Tubeness plugin (sigma = 0.66) (Sato et al., 1998).
377 Finally, images were binarized using the Bernsen's AutoLocal threshold method (radius =

2) (Bernsen, 1986). The resulting binary stack was analyzed first with the 3D Object Counter function to obtain the total neuronal network volume (mm^3). The channel with the gut staining was processed by background subtraction and then thresholder using the Li's method (Li and Lee, 1993). The resulting binary stack was analyzed with the 3D Object Counter function to obtain the volume of the gut.

For other quantifications: The number of Elav/Hoechst positive nuclei in the HCG was counted from the confocal stack using the 3D Object Counter plugin. The number of TTC nuclei was counted by hand from the confocal stack maximum projection. TTCs volume was obtained using the same procedure as for neural tissue quantification. The number of H3P/ Hoechst positive nuclei in the midgut was counted directly under the confocal microscope. For quantification of cumulative proliferation using ReDDM, xyz stacks of half the gut were taken and z-projected. The Hoechst signal was manually outlined to measure the gut area. To quantify the area of GFP signal from mCD8::GFP-labeled cells (representing ISCs and EBs resulting from ISCs divisions) a Gaussian Blur filter (radius = 2.0) was applied. The image was then thresholded using the "MaxEntropy" algorithm (Kapur et al., 1985) and finally, the GFP-positive regions larger than $10\mu m^2$ were quantified. The GFP area was represented as a percentage of the total area.

Other quantifications

For the SMURF assay (Rera et al., 2012), on the 4th day of the DSS feeding protocol, we assessed the proportion of surviving flies that were positive for the SMURF phenotype.

Statistics

Data analysis was carried out using Prism 6 (GraphPad Software Inc., San Diego, CA) and Statgraphics Centurion version 18 (Statgraphics Technologies Inc., The Plains, VA). Experiments were performed with three biological replicates yielding similar results, and a representative replicate is shown. A minimum of 15 guts were analyzed for each condition. For the SMURF assay ten tubes with 10 flies each were used. For data shown in box plots, the median is given between the first and third quartiles (ends of the box). Whiskers represent the maximum and minimum values of the data. Bar graphs display the mean, with error bars representing the standard deviation.

For the amount of neural tissue and TTCs tissue: To analyze the effect of the treatment on neural tissue volume and TTCs tissue volume, analysis of covariance (ANCOVA) was performed. The dependent variable was neural tissue volume or TTCs tissue volume, the fixed factor was the treatment, and the covariate was gut volume (Figure 1B, D, E; Figure 2D, E; Figure 3A, D, E; Supplementary Figure 1B, C; Supplementary Figure 2).

For other quantifications: For pairwise comparisons of data sets following a normal distribution (Figure 1C) the unpaired t-test was performed. For pairwise comparisons of data sets not following a normal distribution we used the non-parametric Mann Whitney test (Figure 2A-C; Supplementary Figure 1A).

FUNDING

This work was funded by the Spanish Ministerio de Ciencia e Innovación (grant PID2019-107340GB-I00) and Agència de Gestió d'Ajuts Universitaris i de Recerca of the Generalitat de Catalunya (2021SGR00293) to M.M. Work in I.M-A. was funded by an ERC Advanced Grant (ERCAdG 787470 "IntraGutSex"), a UKRI Horizon Europe guarantee grant (EPSRC-ERC EP/Y03298/1), MRC intramural funding and the Francis Crick Institute, which receives its core funding from Cancer Research UK (FC001317 and FC001175), the UK Medical Research Council (FC001317 and FC001175), and the Wellcome Trust (FC001317 and FC001175).

ACKNOWLEDGEMENTS

We thank C. González, M. Milán, C. Estella, J. Morante, B. Hudry, M. Corominas, F. Serras, BDSC and DSHB for reagents and members of the Corominas' and Serras' laboratories for insightful discussions. We are grateful to Q. Zhu and O. Ramirez for their assistance with early pilot experiments that helped shape this research. We are indebted to our colleagues F. Cebrià, M. Milán, M. Corominas, F. Serras, B. Payer and the CCiTUB technological platform for their invaluable support and encouragement during this project.

CONFLICT OF INTERESTS

The authors declare that they have no conflict of interest.

CONTRIBUTIONS

Conceptualization: M.M.; Methodology: M.R-M., M.B., P.G., A.M., S.R., I.M-A., M.M.; Investigation: M.R-M., M.M.; Formal Analysis: M.R-M., P.G., A.M., S.R., I.M-A., M.M.; Validation: M.R-M., M.M.; Visualization: M.R-M., M.M.; Data Curation: M.R-M., M.M.; Resources: P.G., A.M., I.M-A.; Supervision: M.M.; Project Administration: M.M.; Funding Acquisition: M.M.; Writing – Original Draft: M.M. with contributions from all the authors.

REFERENCES

Amcheslavsky, A., Jiang, J., Ip, Y.T., 2009. Tissue Damage-Induced Intestinal Stem Cell Division in Drosophila. Cell Stem Cell 4, 49–61. https://doi.org/10.1016/j.stem.2008.10.016

Antonello, Z.A., Reiff, T., Ballesta-Illan, E., Dominguez, M., 2015. Robust intestinal homeostasis relies on cellular plasticity in enteroblasts mediated by miR-8–Escargot switch. EMBO J. 34, 2025–2041. https://doi.org/10.15252/embj.201591517

Bell, L.R., Horabin, J.I., Schedl, P., Cline, T.W., 1991. Positive autoregulation of Sex-lethal by alternative splicing maintains the female determined state in Drosophila. Cell 65, 229–239. https://doi.org/10.1016/0092-8674(91)90157-T

Bell, L.R., Maine, E.M., Schedl, P., Cline, T.W., 1988. Sex-lethal, a Drosophila sex determination switch gene, exhibits sex-specific RNA splicing and sequence similarity to RNA binding proteins. Cell 55, 1037–1046. https://doi.org/10.1016/0092-8674(88)90248-6

Belote, J.M., McKeown, M., Boggs, R.T., Ohkawa, R., Sosnowski, B.A., 1989. Molecular genetics of *transformer* , a genetic switch controlling sexual differentiation in *Drosophila*. Dev. Genet. 10, 143–154. https://doi.org/10.1002/dvg.1020100304

Bentley, D., Toroian-Raymond, A., 1981. Embryonic and postembryonic morphogenesis of a grasshopper interneuron. J. Comp. Neurol. 201, 507–518. https://doi.org/10.1002/cne.902010404

Bernsen, J., 1986. Dynamic Thresholding of Gray Level Image. Proc. Int. Conf. Pattern Recognit. Berl. ICPR 86 1251–1255.

Boggs, R.T., Gregor, P., Idriss, S., Belote, J.M., McKeown, M., 1987. Regulation of sexual differentiation in D. melanogaster via alternative splicing of RNA from the transformer gene. Cell 50, 739–747. https://doi.org/10.1016/0092-8674(87)90332-1

Bucher, D., Pflüger, H.-J., 2000. Directional sensitivity of an identified wind-sensitive interneuron during the postembryonic development of the locust. J. Insect Physiol. 46, 1545–1556. https://doi.org/10.1016/S0022-1910(00)00078-0

Buchon, N., Osman, D., David, F.P.A., Yu Fang, H., Boquete, J.-P., Deplancke, B., Lemaitre, B., 2013. Morphological and Molecular Characterization of Adult Midgut Compartmentalization in Drosophila. Cell Rep. 3, 1725–1738. https://doi.org/10.1016/j.celrep.2013.04.001

Chen, J., Reiher, W., Hermann-Luibl, C., Sellami, A., Cognigni, P., Kondo, S., Helfrich-Förster, C., Veenstra, J.A., Wegener, C., 2016. Allatostatin A Signalling in

Drosophila Regulates Feeding and Sleep and Is Modulated by PDF. PLOS Genet. 12, e1006346. https://doi.org/10.1371/journal.pgen.1006346

Cirillo, C., Brihmat, N., Castel-Lacanal, E., Le Friec, A., Barbieux-Guillot, M., Raposo, N., Pariente, J., Viguier, A., Simonetta-Moreau, M., Albucher, J.-F., Olivot, J.-M., Desmoulin, F., Marque, P., Chollet, F., Loubinoux, I., 2020. Post-stroke remodeling processes in animal models and humans. J. Cereb. Blood Flow Metab. 40, 3–22. https://doi.org/10.1177/0271678X19882788

Cognigni, P., Bailey, A.P., Miguel-Aliaga, I., 2011. Enteric Neurons and Systemic Signals Couple Nutritional and Reproductive Status with Intestinal Homeostasis. Cell Metab. 13, 92–104. https://doi.org/10.1016/j.cmet.2010.12.010

Cui, X., Meiselman, M.R., Thornton, S.N., Yapici, N., 2024. A gut-brain-gut interoceptive circuit loop gates sugar ingestion in Drosophila. https://doi.org/10.1101/2024.09.02.610892

Gao, Z., Pang, Z., Chen, Y., Lei, G., Zhu, S., Li, G., Shen, Y., Xu, W., 2022. Restoring After Central Nervous System Injuries: Neural Mechanisms and Translational Applications of Motor Recovery. Neurosci. Bull. 38, 1569–1587. https://doi.org/10.1007/s12264-022-00959-x

Hérault, C., Pihl, T., Hudry, B., 2024. Cellular sex throughout the organism underlies somatic sexual differentiation. Nat. Commun. 15, 6925. https://doi.org/10.1038/s41467-024-51228-6

Holsopple, J.M., Cook, K.R., Popodi, E.M., 2022. Enteroendocrine cell expression of split-GAL4 drivers bearing regulatory sequences associated with panneuronally expressed genes in Drosophila melanogaster. Open Access.

Howard, A.M., LaFever, K.S., Fenix, A.M., Scurrah, C.R., Lau, K.S., Burnette, D.T., Bhave, G., Ferrell, N., Page-McCaw, A., 2019. DSS-induced damage to basement membranes is repaired by matrix replacement and crosslinking. J. Cell Sci. 132, jcs226860. https://doi.org/10.1242/jcs.226860

Hyer, M.M., Phillips, L.L., Neigh, G.N., 2018. Sex Differences in Synaptic Plasticity: Hormones and Beyond. Front. Mol. Neurosci. 11, 266. https://doi.org/10.3389/fnmol.2018.00266

Inoue, K., Hoshijima, K., Sakamoto, H., Shimura, Y., 1990. Binding of the Drosophila Sex-lethal gene product to the alternative splice site of transformer primary transcript. Nature 344, 461–463. https://doi.org/10.1038/344461a0

Jenett, A., Rubin, G.M., Ngo, T.-T.B., Shepherd, D., Murphy, C., Dionne, H., Pfeiffer, B.D., Cavallaro, A., Hall, D., Jeter, J., Iyer, N., Fetter, D., Hausenfluck, J.H., Peng, H., Trautman, E.T., Svirskas, R.R., Myers, E.W., Iwinski, Z.R., Aso, Y., DePasquale, G.M., Enos, A., Hulamm, P., Lam, S.C.B., Li, H.-H., Laverty, T.R., Long, F., Qu, L., Murphy, S.D., Rokicki, K., Safford, T., Shaw, K., Simpson, J.H., Sowell, A., Tae, S., Yu, Y., Zugates, C.T., 2012. A GAL4-Driver Line Resource for Drosophila Neurobiology. Cell Rep. 2, 991–1001. https://doi.org/10.1016/j.celrep.2012.09.011

Jiang, H., Tian, A., Jiang, J., 2016. Intestinal stem cell response to injury: lessons from Drosophila. Cell. Mol. Life Sci. 73, 3337–3349. https://doi.org/10.1007/s00018-016-2235-9

Kapur, J.N., Sahoo, P.K., Wong, A.K.C., 1985. A new method for gray-level picture thresholding using the entropy of the histogram. Comput. Vis. Graph. Image Process. 29, 273–285. https://doi.org/10.1016/0734-189X(85)90125-2

Kenmoku, H., Ishikawa, H., Ote, M., Kuraishi, T., Kurata, S., 2016. A subset of neurons controls the permeability of the peritrophic matrix and midgut structure in *Drosophila* adults. J. Exp. Biol. jeb.122960. https://doi.org/10.1242/jeb.122960

Kirby, E.D., Andrushko, J.W., Rinat, S., D'Arcy, R.C.N., Boyd, L.A., 2024. Investigating female versus male differences in white matter neuroplasticity associated with complex visuo-motor learning. Sci. Rep. 14, 5951. https://doi.org/10.1038/s41598-024-56453-z

Ksiazek-Winiarek, D.J., Szpakowski, P., Glabinski, A., 2015. Neural Plasticity in Multiple Sclerosis: The Functional and Molecular Background. Neural Plast. 2015, 1–11. https://doi.org/10.1155/2015/307175

Kuraishi, T., Kenmoku, H., Kurata, S., 2015. From mouth to anus: Functional and structural relevance of enteric neurons in the Drosophila melanogaster gut. Insect Biochem. Mol. Biol. 67, 21–26. https://doi.org/10.1016/j.ibmb.2015.07.003

Lee, S., Stevens, C.F., 2007. General design principle for scalable neural circuits in a vertebrate retina. Proc. Natl. Acad. Sci. 104, 12931–12935. https://doi.org/10.1073/pnas.0705469104

Lemaitre, B., Miguel-Aliaga, I., 2013. The Digestive Tract of *Drosophila melanogaster*. Annu. Rev. Genet. 47, 377–404. https://doi.org/10.1146/annurev-genet-111212-133343

Li, C.H., Lee, C.K., 1993. Minimum cross entropy thresholding. Pattern Recognit. 26, 617–625. https://doi.org/10.1016/0031-3203(93)90115-D

Lund-Ricard, Y., Cormier, P., Morales, J., Boutet, A., 2020. mTOR Signaling at the Crossroad between Metazoan Regeneration and Human Diseases. Int. J. Mol. Sci. 21, 2718. https://doi.org/10.3390/ijms21082718

Luo, L., O'Leary, D.D.M., 2005. AXON RETRACTION AND DEGENERATION IN DEVELOPMENT AND DISEASE. Annu. Rev. Neurosci. 28, 127–156. https://doi.org/10.1146/annurev.neuro.28.061604.135632

Mahar, M., Cavalli, V., 2018. Intrinsic mechanisms of neuronal axon regeneration. Nat. Rev. Neurosci. 19, 323–337. https://doi.org/10.1038/s41583-018-0001-8

Mank, J.E., Rideout, E.J., 2021. Developmental mechanisms of sex differences: from cells to organisms. Development 148. https://doi.org/10.1242/dev.199750

Marianes, A., Spradling, A.C., 2013. Physiological and stem cell compartmentalization within the Drosophila midgut. eLife 2, e00886. https://doi.org/10.7554/eLife.00886

McGuire, S.E., Le, P.T., Osborn, A.J., Matsumoto, K., Davis, R.L., 2003. Spatiotemporal Rescue of Memory Dysfunction in *Drosophila*. Science 302, 1765–1768. https://doi.org/10.1126/science.1089035

Menon, K.P., Carrillo, R.A., Zinn, K., 2013. Development and plasticity of the *Drosophila* larval neuromuscular junction. WIREs Dev. Biol. 2, 647–670. https://doi.org/10.1002/wdev.108

Miguel-Aliaga, I., Jasper, H., Lemaitre, B., 2018. Anatomy and Physiology of the Digestive Tract of *Drosophila melanogaster*. Genetics 210, 357–396. https://doi.org/10.1534/genetics.118.300224

Min, S., Oh, Y., Verma, P., Whitehead, S.C., Yapici, N., Van Vactor, D., Suh, G.S., Liberles, S., 2021. Control of feeding by Piezo-mediated gut mechanosensation in Drosophila. eLife 10, e63049. https://doi.org/10.7554/eLife.63049

Murphy, T.H., Corbett, D., 2009. Plasticity during stroke recovery: from synapse to behaviour. Nat. Rev. Neurosci. 10, 861–872. https://doi.org/10.1038/nrn2735

Nudo, R.J., 2003. Functional and structural plasticity in motor cortex: implications for stroke recovery. Phys. Med. Rehabil. Clin. N. Am. 14, S57–S76. https://doi.org/10.1016/S1047-9651(02)00054-2

Olds, W.H., Xu, T., 2014. Regulation of food intake by mechanosensory ion channels in enteric neurons. eLife 3, e04402. https://doi.org/10.7554/eLife.04402

Ollion, J., Cochennec, J., Loll, F., Escudé, C., Boudier, T., 2013. TANGO: a generic tool for high-throughput 3D image analysis for studying nuclear organization. Bioinformatics 29, 1840–1841. https://doi.org/10.1093/bioinformatics/btt276

Oswald, M.C.W., Garnham, N., Sweeney, S.T., Landgraf, M., 2018. Regulation of neuronal development and function by ROS. FEBS Lett. 592, 679–691. https://doi.org/10.1002/1873-3468.12972

Perochon, J., Yu, Y., Aughey, G.N., Medina, A.B., Southall, T.D., Cordero, J.B., 2021. Dynamic adult tracheal plasticity drives stem cell adaptation to changes in intestinal homeostasis in Drosophila. Nat. Cell Biol. 23, 485–496. https://doi.org/10.1038/s41556-021-00676-z

Petersen, E.D., Sharkey, E.D., Pal, A., Shafau, L.O., Zenchak-Petersen, J., Peña, A.J., Aggarwal, A., Prakash, M., Hochgeschwender, U., 2022. Restoring Function After Severe Spinal Cord Injury Through BioLuminescent-OptoGenetics. Front. Neurol. 12, 792643. https://doi.org/10.3389/fneur.2021.792643

Petsakou, A., Liu, Yifang, Liu, Ying, Comjean, A., Hu, Y., Perrimon, N., 2023. Cholinergic neurons trigger epithelial Ca2+ currents to heal the gut. Nature 623, 122–131. https://doi.org/10.1038/s41586-023-06627-y

Prosperini, L., Piattella, M.C., Giannì, C., Pantano, P., 2015. Functional and Structural Brain Plasticity Enhanced by Motor and Cognitive Rehabilitation in Multiple Sclerosis. Neural Plast. 2015, 1–12. https://doi.org/10.1155/2015/481574

Rera, M., Clark, R.I., Walker, D.W., 2012. Intestinal barrier dysfunction links metabolic and inflammatory markers of aging to death in Drosophila. Proc. Natl. Acad. Sci. U. S. A. 109, 21528–21533. https://doi.org/10.1073/pnas.1215849110

Rodríguez, A., Foronda, D., Córdoba, S., Felipe-Cordero, D., Baonza, A., Miguez, D.G., Estella, C., 2024. Cell proliferation and Notch signaling coordinate the formation of epithelial folds in the *Drosophila* leg. Development 151, dev202384. https://doi.org/10.1242/dev.202384

Sampaio-Baptista, C., Sanders, Z.-B., Johansen-Berg, H., 2018. Structural Plasticity in Adulthood with Motor Learning and Stroke Rehabilitation. Annu. Rev. Neurosci. 41, 25–40. https://doi.org/10.1146/annurev-neuro-080317-062015

Sanal, N., Keding, L., Gigengack, U., Michalke, E., Rumpf, S., 2023. TORC1 regulation of dendrite regrowth after pruning is linked to actin and exocytosis. PLOS Genet. 19, e1010526. https://doi.org/10.1371/journal.pgen.1010526

Sato, Y., Nakajima, S., Shiraga, N., Atsumi, H., Yoshida, S., Koller, T., Gerig, G., Kikinis, R., 1998. Three-dimensional multi-scale line filter for segmentation and visualization of curvilinear structures in medical images. Med. Image Anal. 2, 143–168. https://doi.org/10.1016/S1361-8415(98)80009-1

Schindelin, J., Arganda-Carreras, I., Frise, E., Kaynig, V., Longair, M., Pietzsch, T., Preibisch, S., Rueden, C., Saalfeld, S., Schmid, B., Tinevez, J.-Y., White, D.J., Hartenstein, V., Eliceiri, K., Tomancak, P., Cardona, A., 2012. Fiji: an open-source

platform for biological-image analysis. Nat. Methods 9, 676–682. https://doi.org/10.1038/nmeth.2019

Sosnowski, B.A., Belote, J.M., McKeown, M., 1989. Sex-specific alternative splicing of RNA from the transformer gene results from sequence-dependent splice site blockage. Cell 58, 449–459. https://doi.org/10.1016/0092-8674(89)90426-1

Tamamouna, V., Rahman, M.M., Petersson, M., Charalambous, I., Kux, K., Mainor, H., Bolender, V., Isbilir, B., Edgar, B.A., Pitsouli, C., 2021. Remodelling of oxygen-transporting tracheoles drives intestinal regeneration and tumorigenesis in Drosophila. Nat. Cell Biol. 23, 497–510. https://doi.org/10.1038/s41556-021-00674-1

Tedeschi, A., Bradke, F., 2017. Spatial and temporal arrangement of neuronal intrinsic and extrinsic mechanisms controlling axon regeneration. Curr. Opin. Neurobiol. 42, 118–127. https://doi.org/10.1016/j.conb.2016.12.005

Tian, A., Morejon, V., Kohoutek, S., Huang, Y., Deng, W., Jiang, J., 2022. Damage-induced regeneration of the intestinal stem cell pool through enteroblast mitosis in the *Drosophila* midgut. EMBO J. 41, e110834. https://doi.org/10.15252/embj.2022110834

Titos, I., Juginović, A., Vaccaro, A., Nambara, K., Gorelik, P., Mazor, O., Rogulja, D., 2023. A gut-secreted peptide suppresses arousability from sleep. Cell 186, 1382-1397.e21. https://doi.org/10.1016/j.cell.2023.02.022

Turtzo, L.C., McCullough, L.D., 2008. Sex Differences in Stroke. Cerebrovasc. Dis. 26, 462–474. https://doi.org/10.1159/000155983

Weaver, L.N., Ma, T., Drummond-Barbosa, D., 2020. Analysis of Gal4 Expression Patterns in Adult *Drosophila* Females. G3 GenesGenomesGenetics 10, 4147–4158. https://doi.org/10.1534/g3.120.401676

Williams, D.W., Kondo, S., Krzyzanowska, A., Hiromi, Y., Truman, J.W., 2006. Local caspase activity directs engulfment of dendrites during pruning. Nat. Neurosci. 9, 1234–1236. https://doi.org/10.1038/nn1774

Williams, D.W., Truman, J.W., 2005. Cellular mechanisms of dendrite pruning in *Drosophila* : insights from in vivo time-lapse of remodeling dendritic arborizing sensory neurons. Development 132, 3631–3642. https://doi.org/10.1242/dev.01928

Wu, S.-C., Liao, C.-W., Pan, R.-L., Juang, J.-L., 2012. Infection-Induced Intestinal Oxidative Stress Triggers Organ-to-Organ Immunological Communication in Drosophila. Cell Host Microbe 11, 410–417. https://doi.org/10.1016/j.chom.2012.03.004

Yang, C., Merlin, D., 2024. Unveiling Colitis: A Journey through the Dextran Sodium Sulfate-induced Model. Inflamm. Bowel Dis. 30, 844–853. https://doi.org/10.1093/ibd/izad312

Yaniv, S.P., Schuldiner, O., 2016. A fly's view of neuronal remodeling. WIREs Dev. Biol. 5, 618–635. https://doi.org/10.1002/wdev.241

Yu, C., An, Z., Zhao, W., Wang, W., Gao, C., Liu, S., Wang, J., Wu, J., 2015. Sex Differences in Stroke Subtypes, Severity, Risk Factors, and Outcomes among Elderly Patients with Acute Ischemic Stroke. Front. Aging Neurosci. 7. https://doi.org/10.3389/fnagi.2015.00174